Domain boundary engineering

Ekhard Salje [a]; Huali Zhang [a]

[a] Department of Earth Sciences, University of Cambridge, Cambridge CB2 3EQ, UK

PLEASE SCROLL DOWN FOR ARTICLE

Taylor & Francis
Taylor & Francis Group

Domain boundary engineering

Ekhard Salje* and Huali Zhang

*Department of Earth Sciences, University of Cambridge,
Downing Street, Cambridge CB2 3EQ, UK*

We review the idea that domain boundaries, rather than domains, can carry information and act as memory devices. Domains are bulk objects; their large response to changing external fields is related to their change in volume, which implies the movement of domain boundaries. In many cases, the design of 'optimal' domain structures corresponds to 'optimal' domain boundaries with parameters such as the domain boundary mobility, pinning properties and the formation of specific boundaries such as curved boundaries or needle domains. This argument is enhanced further in this review: domain boundaries themselves can host properties which are absent in the bulk, they can be multiferroic, super- or semi-conductors while the matrix shows none of these properties. It is agued that multiferroic walls can be described formally as chiral whereby the chirality relates to state-vectors such as polarisation and magnetic moment and their (non-linear) coupling. Once such walls can be generated reliably, a new generation of devices with much higher storage density than ever produced before can be envisaged.

Keywords: domain boundary; order parameter; multiferroic; chirality; ferroelectricity

1. Introduction

Ferroic phase transitions generate, under the appropriate boundary conditions, domain structures, which often dominate the macroscopic susceptibility of the material. Magnetic, ferroelectric and ferroelastic materials show very large values of their switchable magnetic moment, their polarisation, and their spontaneous strain, respectively, when domain structures change under external fields. The optimisation of the domain structures to generate the largest possible susceptibility has been subject to much research and leads to the formulation of specific domain pattern as collective features. Stripe patterns with a high density of domain walls, needle patterns with wedge-like needle domains, junction patterns with many intersections of domain walls, and tweed patterns were extensively discussed in the literatures [1–7]. In co-elastic materials the strain of the material may be significant, but no switchable domain structures exist [8,9]. This means that in this case all structural deformations occur exclusively in the bulk. The role of incommensurations has been emphasised previously, but will not be discussed here any further [10,11].

*Corresponding author. Email: ekhard@esc.cam.ac.uk

With the re-advent of a wider debate on multi-ferroic materials [12–20] the traditional issue of how one ferroic property can influence or even create another ferroic property becomes important. While a full analysis of experimental situations for bulk materials is still controversial it has become clear [21] that such multi-ferroic behaviour can originate from the internal domain wall structure. The generic case is a ferroelastic material (say $CaTiO_3$) with no other ferroic properties besides ferroelasticity. When this material contains domains and, thus, ferroelastic domain walls, the domain walls themselves can be ferroelectric or ferri-electric - a property which does not exist in the bulk. Similarly, it may be possible to observe magnetic walls in ferroelastic or ferroelectric matrices [22,23]. However, while interfacial properties can generate multiferroic properties [24] one needs to also be careful to avoid trivial artefacts which have nothing to do with multiferroic behaviour at all [25]. With respect to such 'local' properties one observes often that interfaces and walls are not simply the classic interpolation of bulk properties as seen in Landau theory [26,27]. The non-ferroic material zircon serves as an example that undergoes a local transformation into a glassy state when irradiated by radiogenic impurities. The damaged areas have a diameter of ca. 5 nm and are separated from the bulk by an interface of highly polymerised material [28,29]. When the elastic susceptibility of this assembly is measured one finds that the macroscopic sample shows a much stiffer elastic response than one would calculate in the Hashin-Shtrikman approximation of a two phase mixture. The reason for the stiff behaviour is that the interface 'protects' the inner core of the damaged areas and prevents it from stronger compression. Hence the scaling of the elastic response is not that of the bulk proportions of the two phases (as usually assumed) but is strongly modified by the interfacial stress and, thus, shows the additional scaling of the interfaces [30]. This behaviour may be more widespread in other materials where the interfaces or domain walls modify the macroscopic behaviour significantly even when their volume proportion is modest. Static twin boundaries, on the other hand, seem not to generate elastic softening even though their internal density can be much less than that of the bulk [31–33].

These examples show that the internal structure of domain boundaries, interfaces, twin walls etc. can have a significant effect on the macroscopic behaviour of material useful for engineering purposes. This effect can, in specific cases, even outperform the enhanced properties, which come from the optimisation of the domain structure [34]. In this sense one would like to optimise the interfacial properties rather than the domain structure itself. Once this becomes possible we enter into an area where 'domain boundary engineering' may provide answers where the more traditional 'domain engineering' fails or gives only insufficient solutions [35–37]. The term 'engineering' implies that specific domain boundaries can be made which have the desired properties. In this review we focus on properties of domain boundaries as they naturally occur in bulk material rather than MBE-made devices where the interfaces are the result of the growth conditions [24].

2. Chemical doping of domain walls

Before we investigate the intrinsic changes of the crystal structure inside twin walls, we focus on their chemical modifications. Chemical transport along twin walls and grain boundaries is well understood to be different from that of the bulk [38–41]. In general, transport is faster along twin walls (or grain boundaries) so that any modification of the twin wall composition is relatively easily achieved when the sample is exposed to external chemical agents. These can then diffuse and equilibrate along the walls while the bulk

remains relatively unaffected. In material sciences of ferroic materials we have examples where small amounts of Na were injected into WO_3 (Figure 1a and b). As a result, the composition of the twin walls changed from WO_3 to Na_xWO_3 or WO_{3-x} which are for certain values of x superconducting phases [42–44]. Indeed, these twin walls became superconducting while the bulk remained an insulator (Figure 2).

The enrichment of domain walls with chemical species is a well-known phenomenon in mineralogy and geo-chemistry. Careful chemical analysis using analytical transmission electron microscopy [45] showed that, e.g., twin boundaries in feldspars preferentially
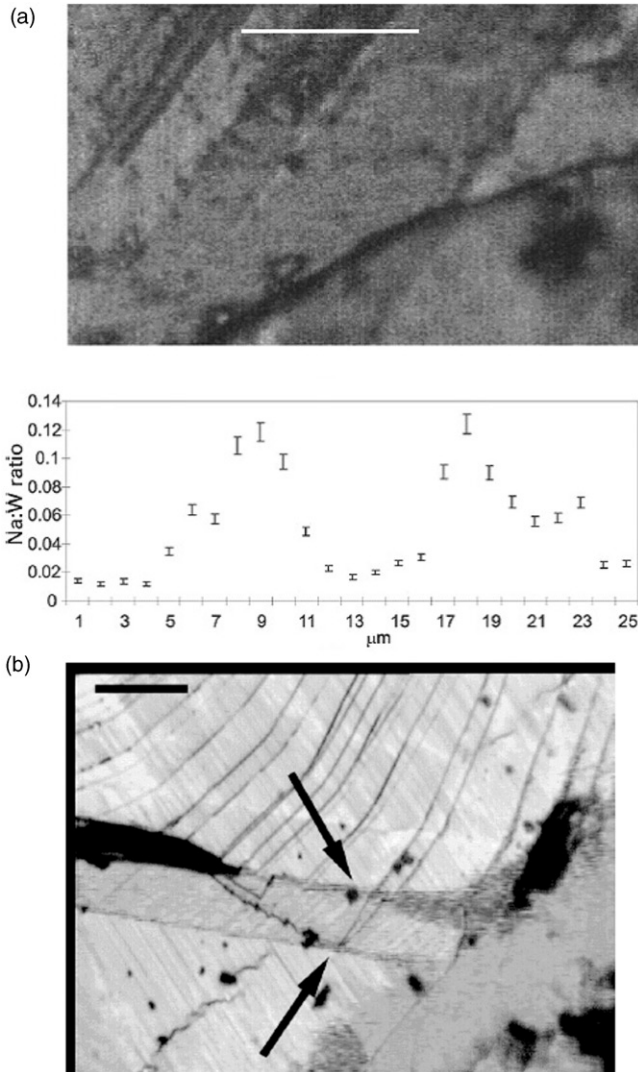
Figure 1. (a) Twinned crystal of WO_3, with domains from the tetragonal-orthorhombic phase transition. The white line (length $= 25\,\mu m$) shows the line scanned in the microprobe analysis which shows that the Na ions are preferentially located along the twin walls. (b) macroscopic sample with two parallel twin walls loaded with traces of Na. These walls are superconducting (Figure 2). The scale bar in the top left corner is $50\,\mu m$.
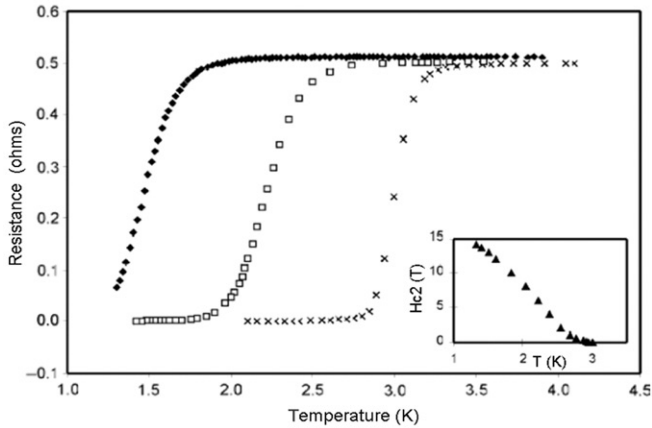
Figure 2. Resistivity of the sample shown in Figure 1(b) with two parallel domain walls over an extended temperature interval. The onset of superconductivity in the walls is at 3.2 K. The magnetic fields are $0\,T$ (×), $6\,T$ (□) and $13\,T$ (♦). The inset shows the temperature dependence of H_{c2}.

attract alkali atoms and are depleted in Ca and Al leading to shape memory effects [46]. The connection between shape memory effects and mobile atomic species was also postulated for alloys [47–50] although Otsuka and Ren [51] argued that strain related ordering inside the domains rather than the pinning of the domain boundaries leads to aging and shape memory effects in some alloys. This idea was extended [52,53] whereby the wall pinning at the interface between two different atomic ordering schemes can still not be excluded.

It is important to note that transport can also be reduced in twin walls for specific materials. Such a case is related to the transport of Na^+ and Li^+ through a quartz crystal with {100} Dauphine twinning [54]. Computer simulation showed that the transport rate along the twin walls was reduced for the [0 0 1] channels. This effect is related to the local structure of quartz at the twin boundary; structural continuity across the twin boundary requires that the [0 0 1] channels are more distorted in the twin wall than in the bulk material while the volume of the channels increases. This increase goes together with a decrease of the minimum diameter of the channels which, ultimately, limits the transport. The probably most common doping in perovskite oxides relates to oxygen vacancies. Significant pinning of the movement of twin boundaries by oxygen vacancies occurs in polycrystalline $Ca_{1-x}Sr_xTiO_3$ and $LaAlO_3$ single crystals [55,56]. The activation energy for domain wall motion (determined from the temperature and frequency dependence of the storage modulus and loss tangent), is of the order of 0.88–1.09 eV, which is comparable with the activation energy for O-atom diffusion through a perovskite structure. Lagraff and Payne [57] found that the ferroelastic domain mobility in $YBa_2Cu_3O_{7-\delta}$ was also constrained by O-atom mobility, and simulations by Calleja et al. [58] found that O-atom vacancies were stabilised on twin boundaries in $CaTiO_3$, with a saddle point energy of 1.2 eV. The accumulation of such defects as discussed in much detail heavily influences the thickness of the domain [59–61].

The equivalent effect is much weaker in fluorides. In improper ferroelastic $KMnF_3$ and $KMn_{1-x}Ca_xF_3$, the an-elastic softening related to the movement of twin boundaries below the cubic-tetragonal phase transition is very strong [62]. Very weak pinning of the walls was observed with a fairly narrow distribution of activation energies near 0.42 eV.

Wall movements in Ca-doped samples are best described by Vogel-Fulcher relaxations with a characteristic energy of 0.23 eV. The activation energies are related to interaction between F vacancies or interstitials and the moving domain walls; additional Ca doping appears to increase the tendency to form glass-like states. No domain freezing occurs at temperatures above the phase transition I4/mcm–Pnma at lower temperatures; the Pnma phase does not show any domain movement or anelastic behaviour [62].

In summary, chemical modifications of twin walls are very common, even when they are not intended and occur by accident. Deliberate doping can lead to new compounds along the walls while defects accumulate in case of oxygen vacancies while the equivalent fluorene vacancies are less common or less significant for the pinning of twin walls. Finally, a very exciting new development for the self-pinning of twin walls and interfaces was postulated several authors involving the spontaneous generation of dislocations by the moving interface. The role of the dislocations is then to hinder exactly this movement and lead to shape memory behaviour [63]. Experimental observation on the role of dislocations together with the presence of hydrogen can be found in a recent paper [64]. In Shape Memory Alloys (SMA) equivalent studies of pinning processes of domain walls and their effect on aging has been clearly identified [65–67], in particular the role of dislocations during the first order martensitic transition [64,68,69].

3. Structural modifications of twin walls: the role of the secondary order parameter

The main advance made in the understanding of the internal structure of domain boundaries in solids is the realisation that structural changes inside walls do not follow the simple concept of the Landau–Ginzburg theory for one order parameter – even when the chemical composition is not changed. Before we discuss in detail, let us first recall the traditional concept of a single-order parameter treatment. The profile of $Q(x)$ across a twin wall is found by minimisation of the Gibbs free energy

$$G(Q, T) = \frac{1}{2} A/\theta_s (\coth(\theta_s/T) - \coth(\theta_s/T_c))Q^2 + \frac{1}{4}BQ^4 + \frac{1}{6}CQ^6 + \frac{1}{2}g(\nabla Q)^2 \qquad (1)$$

where T_c is the Curie temperature, θ_s is the quantum mechanical saturation temperature. A, B, C and g are appropriate energy parameters which may either be determined experimentally [68,70–75] or follow from energy calculations. The minimisation is usually performed via solving the time-dependent Euler–Lagrange equation in the steady state

$$\partial Q/\partial t = -A/\theta_s(\coth(\theta_s/T) - \coth(\theta_s/T_c))Q - BQ^3 - CQ^5 + g(\nabla^2 Q) = 0 \qquad (2)$$

The well-known answer for the boundary conditions of a kink ($Q = -Q_{max}$ for $x = -\infty$ and $Q = Q_{max}$ for $x = \infty$) is $Q = Q_{max} \tanh(x/w)$. The total wall thickness is 2w with

$$w = (2g\theta_s/A(\coth(\theta_s/T) - \coth(\theta_s/T_c)))^{1/2} \qquad (3)$$

which simplifies at high temperatures to the well known Landau-Ginzburg dependence

$$w = (2g/A(T - T_c))^{1/2} \qquad (4)$$

The wall energy increases very weakly when lowering the temperature through the transition point [76].

There are few experimental observations which confirm these results; probably the most extensive study is by Chrosch and Salje [77] who measured the wall thickness in LaAlO$_3$ as a function of temperature over a very large temperature interval [78–87].

An excellent attempt to measure the wall thickness in a SMA using direct AFM methods was undertaken recently by Shilo et al. [70]. The wall thickness was found to be 0.7 nm. While the error in such determinations is large they show that the walls are rather akin to (but thinner than) ferroelastic walls in non-metallic materials. The wall energy was accordingly estimated to be $70 \, \text{mJ} \, \text{m}^{-2}$ which is again similar to wall energies in ferroelastics. A similar estimate for Ni-Ti-Fe alloys [71] found an estimate of $14 \, \text{mJ} \, \text{m}^{-2}$ for this compound.

For any complex structure, however, this simple approach to describe the structural deformations is bound to fail while the experimentally observable temperature dependence of the wall thickness may not change significantly. The issue is that the change of the order parameter Q inside the wall will virtually always trigger secondary changes of other structural parameters. A typical example is the rotation of octahedra in perovskite structures [88]. Each rotation will be accompanied by a volume change simply because each twist of two adjacent octahedral will approach the centres of the octahedra, an effect which preoccupied Helen Megaw already in 1946 [89] and was discussed further by Glazer [90].

In reality, octahedra do not remain rigid but distort during the rotation. A symmetry problem remains, however: the symmetry of the rotation representing the order parameter is given by the active representation, while the volume change is given by the identity representation. This means that any calculation of the change of the rotation performed under the symmetry constraints of the active representation will automatically ignore the volume change. This makes clearly no sense if the consequence of the change of the volume is actually more important for the physical and chemical behaviour of the twin wall than the rotation. Lee and collaborators have argued that it is virtually impossible for any complex structure to be described by one-order parameter [91]. In general the following couplings to other structural parameters appear plausible:

(1) The domain-wall structure may be strained with respect to the bulk structure. For instance, a positive dilatational strain, perpendicular to the domain wall, will result in the domain-wall structure being more open than the bulk structure allowing atoms to pass through more easily.

(2) The domain wall may have different elastic properties from the bulk material. The existence of phase transitions in ferroelastic materials relies on those materials showing non-linear elastic properties. These non-linearities will strongly affect some of the elastic constants in the bulk. A diffusing atom will cause local distortions of the crystal lattice as it hops from site to site, and the energies associated with the distortion will depend on the elastic constants.

(3) The domain wall may be charged. This is possible in, for example, the case of a ferroelectric domain wall. The diffusion of charged species through the domain wall will be strongly affected by the electrical potential of the wall.

The strains in the domain wall can be determined by the condition that the stresses conjugate to these strain components must be zero. It does not, however, follow from this that the stress tensor is zero in the wall: stresses conjugate to the components of the strain tensor that must remain fixed in the wall will, in general, take non-zero values in the wall, although they must tend toward zero in the bulk [91]. The possible twin planes of a ferroelastic microstructure are determined using the strain compatibility relation $x^T(\varepsilon_1 - \varepsilon_2)x = 0$, where ε_1 and ε_2 are the spontaneous strains of two domains, and x is a vector lying in the plane of the domain wall [91]. This equation is usually used to calculate the possible values of x and, thus, the plane of the domain wall. However, once

the plane of the domain wall is known, the equation may be written in the form $x^T(\varepsilon_1 - \varepsilon)x = 0$, where ε is the strain at some point inside the domain wall. In this equation, ε_1 and x are already known, so the general form of the strain tensor allowed in the wall can be determined. In computer simulations [91–93] it became apparent that the non-symmetry breaking dilation plays a major role in all materials virtually.

In a one-dimensional approximation, equivalent to the approach in [94] to explain Q–P coupling and leaving aside the compatibility relation and the anisotropy of secondary strains, we can formulate the role of the generalised strain e in the simplest possible model as

$$\Phi(Q, T) = \int \left[\frac{1}{2}aQ^2 + \frac{1}{4}bQ^4 + \frac{1}{2}ce^2 + \lambda Q^2 e + \frac{1}{2}g_1(\partial Q/\partial x)^2 + \frac{1}{2}g_2(\partial e/\partial x)^2 \right] \mathrm{d}x \quad (5)$$

The order parameter is taken here for simplicity to follow a 2-4 Landau potential while the strain enters via the quadratic elastic energy. The coupling between the strain and the order parameter is linear-quadratic in this rather general model. Other coupling terms occur only for specific symmetry conditions. The dispersion terms are different for the order parameter and the strain because, in general, $g_1 \neq g_2$. Changing the scales of Q and e to Φ and ε leads to the scale invariant form with the steady state Euler–Lagrange equations

$$-(1 + 2\lambda)\Phi + \Phi^3 + 2\lambda\Phi\varepsilon = \partial^2\Phi/\partial x^2 \quad (6)$$

and

$$-\lambda\varepsilon + \lambda\Phi^2 = g(\partial^2\varepsilon/\partial x^2) \quad (7)$$

where we consider $g = g_2/g_1 \ll 1$. The simultaneous solution of the two equations is non-trivial unless $g = 0$. In this case the strain is slaved by the (renormalised) order parameter $\varepsilon = \Phi^2$. The new order parameter is $\Phi = \tanh(x/w)$ with $w^2 = 2/(1 + 2\lambda)$ while the strain shows an inverse breather-type singularity, i.e. it reduces from unity outside the wall to zero inside the wall. Increasing coupling strength will decrease the wall width. If g is non-zero but small, perturbation theory can be attempted where changes in ε are larger than those in Φ. An elegant approximation can be found using the trial function $\varepsilon = \Phi^2 + \Delta$ where the correction is given by $\Delta = A(1 - \tanh x/v)$ with the new wall width $v \ll w$. The differential equation for the correction then becomes

$$-\lambda\Delta = g(\partial^2\Delta/\partial x^2) + 2g/w^2[1 - 4\tanh^2(x/v) + 3\tanh^4(x/v)] \quad (8)$$

With $g = 0.1$, $\lambda = 1.1$ one finds an excellent fit for $v/w = 0.35$. The effect of the correction term is to slightly reduce the value of e at $x = 0$, i.e. the breather becomes slightly shallower than in the slaved case with $\varepsilon = \Phi^2$ (Figure 3).

The general observation that the order parameter has a tanh-profile and the strain has a breather-type profile also holds for all other secondary parameters such as charges where e is replaced by P with the same quadratic form of the self energy as in Equation (5). Experimentally this situation relates to $90°$ and $180°$ domains in $BaTiO_3$ and related materials [95–97]. While the dominant secondary effect is the strain coupling in $90°$ walls one finds that the situation in $180°$ walls is more complex. These walls exist with polarisation vectors either in head to tail configuration or in anti-parallel arrangements. The former implies charged walls while the latter has no additional charges in the wall. Other orientations of walls can then be constructed as combinations of these two basic types. It is normally argued that the charged $180°$ walls are
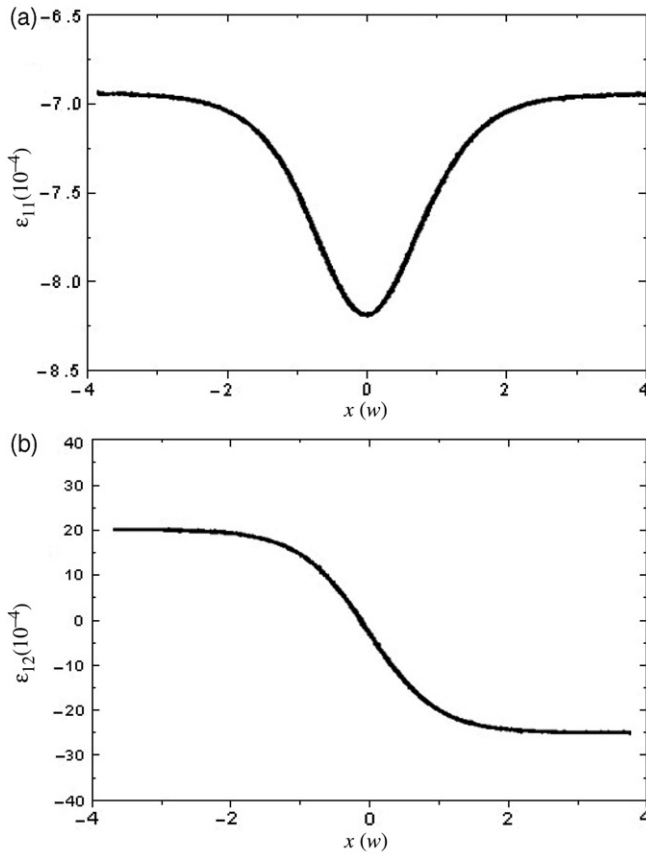
Figure 3. Graphs showing the primary and secondary order parameter in V_3Si. The primary order parameter in (b) follows the $\tanh(x/w)$ – profile while the dilatational strain in (a) shows the typical inverted breather profile (after [91]).

energetically very unstable with respect to the uncharged walls but, nevertheless, both types have been observed in transmission electron microscopy. Careful analysis of the high-resolution images revealed the same situation as envisaged in our treatment: $90°$ walls in $BaTiO_3$ and $PbTiO_3$ are rather thick with significant strain contrast [98,99]. The same is true for charged $180°$ walls in $PbZr_{0.2}Ti_{0.8}O_3$ where the wall thickness was determined from the observed wall profile with $w = 5$ unit cells, approximately. The breather feature was clearly observed for the deformation both in the crystallographic a and c direction. The width of the breather is, within experimental resolution, the same as that of the kink. This indicates that the coupling is significant with the strain while the dipole moment may have additional coupling. Direct observation was reported using piezoelectric response hysteresis in the case of $90°$ walls [100]. In this very elegant work the domain walls in $PbZr_{0.2}Ti_{0.8}O_3$ were swept by an electric field in a piezoresponse force microscope. The piezoresponse signal is proportional to the normal component of the local polarisation. When the domain wall was driven so that the switch between a and c domain happened under the detector, a spike in the polarisation was observed, fully in agreement with arguments given here and, for the case of ferroelectric domains by Ishibashi et al. [96].

4. The case of polar domain walls in a non-polar matrix

Before we discuss the modification of twin walls when two order parameters interact, we recur to a recent study Goncalves-Ferreira et al. [21]. These authors explored the idea that all TiO_6-based perovskite structure may have a tendency to possess polar walls even when the bulk of the material is non-polar (Figure 4). The fundamental idea relates simply to the instability of Ti inside any oxygen octahedron of sufficient size to remain in the centre of the octahedron. It is easy to visualise that an energy minimum exists in such structures in which Ti forms bonds with a subset of oxygen atoms at the expense of the remaining atoms. If Ti forms a bond with one oxygen atom the octahedron suffers tetragonal deformation. Equivalently, bonding with 2 (3) oxygen would lead to an orthorhombic (trigonal) deformation. In a structure this tendency can be compensated by the next nearest neighbour interactions and, while the details of the force balance for Ti can be complex, it may lead to a high symmetry phase at high temperatures. In domain walls, on the other hand, such constraints are limited because the local symmetry is broken anyway and new secondary order parameters become possible. This scenario goes beyond the order parameter/strain coupling as discussed so far and requires two structural instabilities which couple according to their respective symmetry rules. This coupling is best visualised in the so-called order parameter vector space which has been used for several cases. A convenient way to depicture such mixed state of multiferroics or degenerate order parameter is to construct the order parameter vector space [1,101–103]. In this construction, each state parameter defines a subspace of dimension n (the degeneracy of the order parameter, i.e. the dimensionality of the active representation) in which this state is described. The space averaged order parameter component has always the dimension one and values between 0 for the paraphase and 1 in the classic limit of zero temperature. Taking into account the quantum saturation this value is always less than one but the parameter space is usually depicted in the interval [0,1] for each subspace. Each subspace with reduced dimensionality to 1 is now represented as a vector so that the total order parameter vector space has the dimension $\sum n_i$ where the sum is taken over all order parameters considered. To exemplify the procedure we take two one-dimensional representations which form a two dimensional order parameter vector space. The state of the system is then described in this vector space by a resulting vector which can, if both order parameters are independent, simply the vector sum of the two base vectors (Figure 5). The interesting case is now that the order parameters are coupled in some well-defined way. Three cases are particularly interesting, namely the bi-linear case (Q_1, Q_2) [104], the linear-quadratic coupling as in the case of the order parameter strain coupling [10,11]. The third and more complex case is the bi-quadratic case $(Q_1^2 Q_2^2)$ where minimisers can be derived from the Landau potential [105,106]

$$G(Q_1, Q_2, T) = \frac{1}{2} A(T - T_c)Q_1^2 + \frac{1}{4}BQ_1^4 + \frac{1}{6}CQ_1^6 + \frac{1}{2}g(\nabla Q_1)^2 + \frac{1}{2}A'(T - T_c')Q_2^2 + \frac{1}{4}B'Q_2^4$$
$$+ \frac{1}{6}C'Q_2^6 + \frac{1}{2}g'(\nabla Q_2)^2 + \lambda Q_1^2 Q_2^2 \tag{9}$$

Solutions for $dG/dQ_1 = dG/dQ_2 = 0$ were discussed previously for the uniform case [1]. They involve 3 states, namely

$$Q_1 = 0, \ Q_2 \neq 0 \quad \text{and} \quad Q_1 \neq 0, \ Q_2 = 0 \quad \text{and} \quad Q_1 \neq 0, \ Q_2 \neq 0 \tag{10}$$
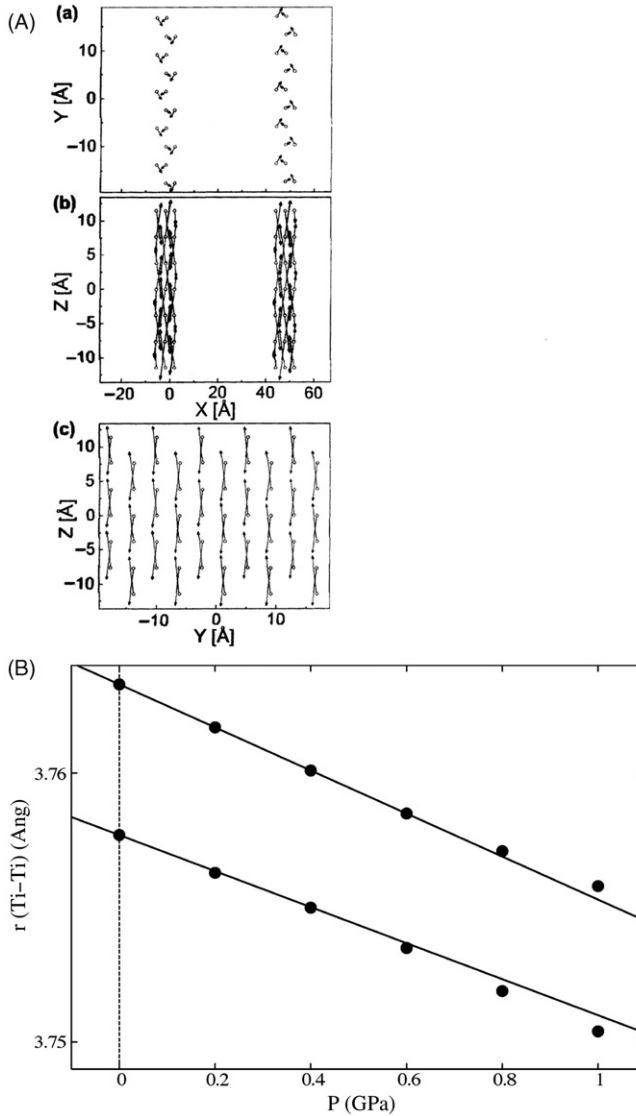
Figure 4. Dipole moments and atomic displacements of Ti inside twin walls of $CaTiO_3$, as projected on to (a) the *xy*, (b) the *xz* and (c) the *yz* planes [19]. The arrows indicated the Ti displacement from the center of the corresponding O octahedron. Their sizes have been scaled by a factor of 300 with respect to the scale in the axes. Part (c) shows the twin wall plane. The gray arrows indicate the direction of the net polarisation. The compressibility of the twin wall is compared with that of the bulk in (b). The Ti–Ti distances in the wall are larger and shown as the upper curve while the Ti–Ti distances in the bulk are smaller in the lower curve. The slopes represent the respective compressibilities. It is seen that the wall compressibility is slightly greater than the bulk compressibility.
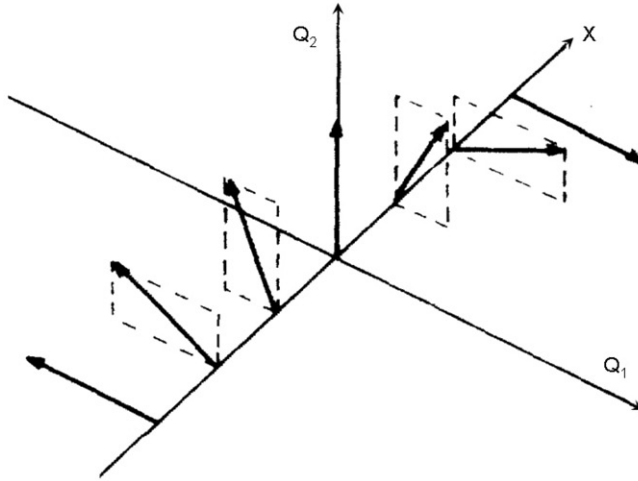
Figure 5. Evolution in space of two-order parameters in the order parameter vector space. Each one-dimensional order parameter spans one dimension in the basal plane. The resulting vector sum represents the structural state of the wall. In the depicted case the order parameter Q_1 (horizontal) changes from $+1$ to -1 while the (secondary) order parameter Q_2 changes from zero to 1 and back to zero. This wall is called chiral. It has two degenerate solutions, namely the order parameter Q_2 changing via a right turn (via the positive maximum value) or a left turn (via the negative maximum value).
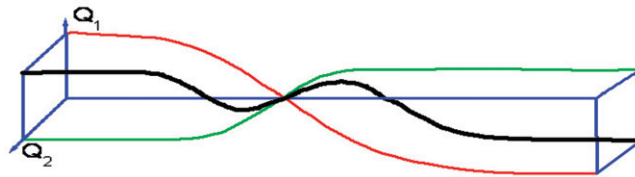

Figure 6. Sketch of bi-chiral wall. The two-order parameters Q_1 and Q_2 are plotted as orthogonal vectors on the left-hand side. The bi-chiral wall is the vector sum $Q_1 + Q_2$ of two primary kinks in Q_1 and Q_2 with two different wall thicknesses $w \neq w'$. The resulting wall profiles are shown as bold curve.

While the uniform solutions are well understood, the non-uniform solutions were first discussed by Houchmanzadeh et al. [107], but not pursued further. Here we discuss some solutions which can be derived by simple perturbation of the equilibrium uniform state.

Two types of solutions are important in the context of this review. The first solution relates to the boundary conditions Q_1, $Q_2 = -1$ at $-\infty$ and Q_1, $Q_2 = 1$ at $+\infty$. For $C = C' = 0$ the solutions for $\lambda = 0$ is again $Q_1 = Q_{10} \tanh(x/w)$ and $Q_2 = Q_{20} \tanh((x - d)/w')$. In general we will find $w \neq w'$ that this solution is bi-chiral (Figure 6) for $d = 0$ in the sense of Houchmanzadeh et al. [107]. In space the state vector follows first more closely one-order parameter and then the second. In the projection of the order parameter vector space (Figure 7) this solution is a curved line through the origin. Linearity occurs when $w = w'$. The solution for negative λ leans that the overlap integral $\lambda \int Q_{12}(r)Q_{22}(r - d)dr$ has a minimum for $d = 0$ so that the two 'solitary wave' solutions attract each other. If, on the other hand, λ is positive but small (weak repulsive coupling between the order parameters) the overlap integral has to be minimised over a large but
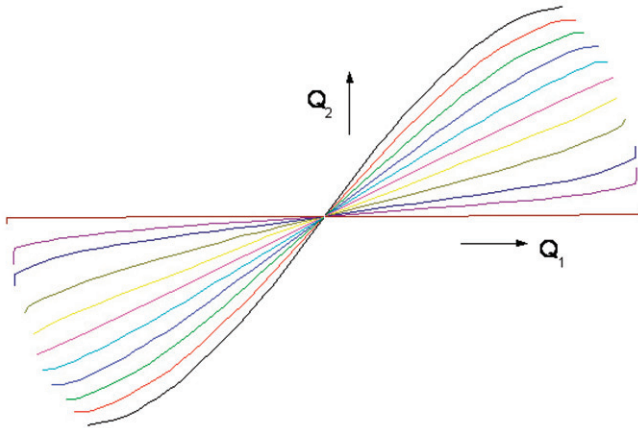
Figure 7. Trajectories of the kink wall profiles for different values of the temperature-related model parameter A'. (A' changes from 0.2 (horizontal line) to -0.4 in steps of 0.1, then from -0.6 to -2 (steepest curve) in steps of 0.2).
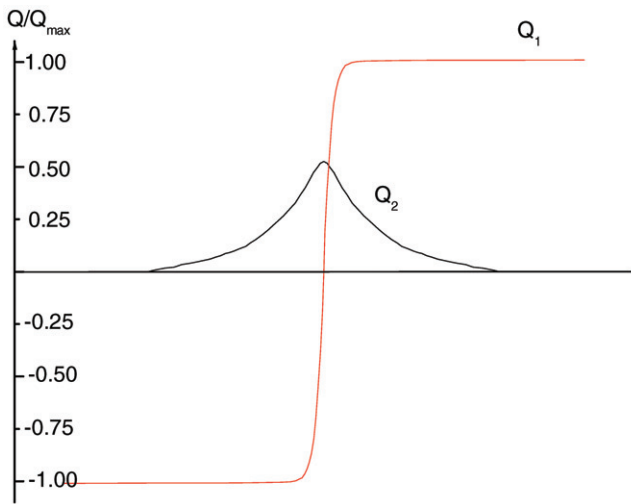

Figure 8. Wall profiles within the marginal stability of phase III ($A' = -0.2$, $Q_1 \neq 0$, $Q_2 \neq 0$,). The bulk material on either side is in phase I ($A' = -0.2$, $Q_1 \neq 0$, $Q_2 = 0$). The wall is the combination of a kink (Q_1) and a breather (Q_2) and is chiral.

finite sample size and leads to a repulsion between the two boundaries. For general values of λ and finite sample size the solution is not yet known.

Other solutions exist for the boundary conditions for one-order parameter to be the same as in the first case but the second-order parameter vanishes for large values of $|r|$ (breather-type solution) (Figure 8). This is exactly the case where the one of the order parameters exists essentially in and near the wall but is reduced anywhere else. This wall has simple chirality [107] where the phase between the two-order parameters defines the sign of the chirality. In perturbation theory the kink-type order parameter, say Q_1 is minimised with the second-order parameter put to zero. The resulting profile is $\tanh(x/w)$

which is then taken as invariant in the coupled equation. The governing equation for Q_2 can be written as

$$G(Q_2, T) = \frac{1}{2} A'(T - T_c')Q_2^2 + \frac{1}{4} B'Q_2^4 + \frac{1}{2}g'(\mathrm{grad}Q_2)^2 + \lambda Q_{10}^2 \tanh(x/w)Q_2^2 \qquad (11)$$

which renormalises the transition temperature to

$$T_c'^* = T_c' - \frac{2\lambda Q_{10}^2}{A'}\tanh(x/w) \qquad (12)$$

which for $T_c' < 2\lambda Q_{10}^2/A'$ suppresses the order parameter Q_2 in the bulk. This case holds for repulsive coupling $\lambda > 0$ while for attractive coupling $\lambda < 0$ the same breather-type solutions remains correct. It is interesting to note that for attractive coupling the breather is a positive function on the uniform order parameter while for attractive coupling the breather is negative (see also calculations by Lee et al. [91]). In either case, the 'secondary order parameter' Q_2 is concentrated (diluted) inside the domain wall while either suppressed or reduced (enhanced) inside the bulk for repulsive (attractive) coupling. Solutions for larger values of the coupling parameter are not yet known. Purely kinetic coupling, where equilibrium conditions do not apply, were earlier discussed in [108] while applications to polytypism were given in [109]. These areas are outside the scope of this review but will certainly be of interest once the details of the generation of specific domain walls is better understood.

Acknowledgements

References

[1] E.K.H. Salje, *Ferroelastic and Co-elastic Crystals*, Cambridge University Press, Cambridge, 1993.

[2] E.K.H. Salje, *Mesoscopic twin patterns in ferroelastic and co-elastic minerals: transformation processes in minerals*, Rev. Mineral. Geochem. 39 (2000), pp. 65–84.

[3] U. Bismayer, J. Hensler, E. Salje, and B. Güttler, *Renormalization phenomena in Ba-diluted ferroelastic lead phosphate $(Pb_{1-x}Ba_x)_3(PO_4)_2$*, Phase Transit. 48 (1994), pp. 149–168.

[4] U. Bismayer, D. Mathes, D. Bosbach, A. Putnis, G. Van Tendeloo, J. Novak, and E.K.H. Salje, *Ferroelastic orientation states and domain walls in lead phosphate type crystals*, Mineral. Mag. 64 (2000), pp. 233–229.

[5] E.K.H. Salje and Y. Ishibashi, *Mesoscopic structures in ferroelastic crystals: needle twins and right-angled domains*, J. Phys.: Condens. Matter 8 (1996), pp. 8477–8495.

[6] E.K.H. Salje, A. Buckley, G. Van Tendeloo, Y. Ishibashi, and G.L. Nord, *Needle twins and right-angled in minerals: comparison between experiment and theory*, Am. Mineral. 83 (1998), pp. 811–822.

[7] E.K.H. Salje, U. Bismayer, S.A. Hayward, and J. Novak, *Twin walls and hierarchical mesoscopic structures*, Mineral. Mag. 64 (2000), pp. 201–212.

[8] D. Speer and E. Salje, *Phase transitions in langbeinites I: crystal chemistry and structures of K-double sulfates of the langbeinite type $M_2^{++} K_2(SO_4)_3$, M^{++}=Mg, Ni, Co, Zn, Ca*, Phys. Chem. Minerals 13 (1986), pp. 17–24.

[9] E.K.H. Salje, A. Ridgwell, B. Güttler, B. Wruck, M.T Dove, and G. Dolino, *On the displacive character of the phase transition in quartz: a hard-mode spectroscopy study*, J. Phys.: Condens. Matter 4 (1992), pp. 571–577.

[10] A.E. Jacobs, D. Mukamel, and D.W. Allender, *Surface states in nearly modulated systems*, Phys. Rev. E 63 (2001), 021704.

[11] A.E. Jacobs, D. Mukamel, and D.W. Allender, *Novel surface state in a class of incommensurate systems*, Phys. Rev. E 61 (2000), pp. 2753–2758.

[12] Y.K. Jun, W.T. Moon, C.M. Chang, H.S. Kim, H.S. Ryu, J.W. Kim, K.H. Kim, and S.H. Hong, *Effects of Nb-doping on electric and magnetic properties inmulti-ferroic BiFeO$_3$ ceramics*, Solid State Commun. 135 (2005), 185401.

[13] B.F. Yu, M.Y. Li, J. Wang, L. Pei, D.Y. Guo, and X.Z. Zhao, *Enhanced electrical properties in multiferroic BiFeO$_3$ ceramics co-doped by La^{3+} and V^{5+}*, J. Phys. D: Appl. Phys. 41 (2008), 185401.

[14] V.A. Stephanovich, M.D. Glinchuk, and R. Blinc, *Magnetoelectric effect in mixed-valency oxides mediated by charge carriers*, Europhy. Lett. 83 (2008), 37004.

[15] P. Padhan, P. LeClair, A. Gupta, and G. Srinivasan, *Magnetodielectric response in epitaxial thin films of multiferroic Bi$_2$NiMnO$_6$*, J. Phys.: Condens. Matter 20, (2008), 355003.

[16] M.P. Cruz, Y.H. Chu, J.X. Zhang, P.L. Yang, F. Zavaliche, Q. He, P. Shafer, L.Q. Chen, and R. Ramesh, *Strain control of domain-wall stability in epitaxial BiFeO$_3$ (110) films*, Phys. Rev. Lett. 99 (2007), 217601.

[17] Y.H. Chu, T. Zhao, M.P. Cruz, Q. Zhang, P.L. Yang, L.W. Martin, M. Huijben, C.H. Yang, F. Zavaliche, H. Zheng, and R. Ramesh, *Ferroelectric size effects in multiferroic BiFeO$_3$ thin films*, Appl. Phys. Lett. 90 (2007), 252906.

[18] R. Ramesh and N.A. Spaldin, *Multiferroics: progress and prospects in thin films*, Nat. Mater. 6 (2007), pp. 21–29.

[19] H. Zheng, J. Wang, S.E. Lofland, Z. Ma, L. Mohaddes-Ardabili, T. Zhao, L. Salamanca-Riba, S.R. Shinde, S.B. Ogale, F. Bai, D. Viehland, Y. Jia, D.G. Schlom, M. Wuttig, A. Roytburd, and R. Ramesh, *Multiferroic BaTiO$_3$-CoFe$_2$O$_4$ nanostructures*, Science 303 (2004), pp. 661–663.

[20] J. Wang, J.B. Neaton, H. Zheng, V. Nagarajan, S.B. Ogale, B. Liu, D. Viehland, V. Vaithyanathan, D.G. Schlom, U.V. Waghmare, N.A. Spaldin, K.M. Rabe, M. Wuttig, and R. Ramesh, *Epitaxial BiFeO$_3$ multiferroic thin film heterostructures*, Science 299 (2003), pp. 1719–1722.

[21] L. Goncalves-Ferreira, S.A.T. Redfern, E. Artacho, and E.K.H. Salje, *Ferrielectric twin walls in CaTiO$_3$*, Phys. Rev. Lett. 101 (2008), 097602.

[22] W. Eerenstein, N.D. Mathur, and J.F. Scott, *Multiferroic and magnetoelectric materials*, Nature 442 (2006), pp. 759–765.

[23] N. Hur, S. Park, P.A. Sharma, J.S. Ahn, S. Guha, and S.W. Cheong, *Electric polarization reversal and memory in a multiferroic material induced by magnetic fields*, Nature 429 (2004), pp. 392–395.

[24] A. Posadas, J.B. Yau, C.H. Ahn, J. Han, S. Gariglio, K. Johnston, K.M. Rabe, and J.B. Neaton, *Epitaxial growth of multiferroic YMnO$_3$ on GaN*, Appl. Phys. Lett. 87 (2005), 171915.

[25] G. Catalan and J.F. Scott, *Magnetoelectrics – is CdCr$_2$S$_4$ a multiferroic relaxor?* Nature 448 (2007), pp. E4–E5.

[26] E.K.H. Salje, *Application of Landau theory for the analysis of phase transitions in minerals*, Phys. Rep. 215 (1992), pp. 49–99.

[27] E.K.H. Salje, S.A. Hayward, and W.T. Lee, *Ferroelastic phase transitions: structure and microstructure*, Acta Cryst. A 61 (2005), pp. 9–18.

[28] I. Farnan and E.K.H. Salje, *The degree and nature of radiation damage in zircon observed by ^{29}Si nuclear magnetic resonance*, J. Appl. Phys. 89 (2001), pp. 2084–2090.

[29] E.K.H. Salje, J. Chrosch, and R.C. Ewing, *Is ''metamictization'' of zircon a phase transition*, Am. Mineral. 84 (1999), pp. 1107–1116.

[30] E.K.H. Salje, *Elastic softening of zircon by radiation damage*, Appl. Phys. Lett. 89 (2006), 131902.

[31] E.K.H. Salje, *An empirical scaling for averaging elastic properties including interfacial effects*, Am. Mineral. 92 (2007), pp. 429–432.

[32] E.K.H. Salje, *(An)elastic softening from static grain boundaries and possible effects on seismic wave propagation*, Phys. Chem. Minerals 35 (2008), pp. 321–330.

[33] L. Goncalves-Ferreira, S.A.T. Redfern, and E. Artacho, *The intrinsic elasticity of twin walls in ferroelastic CaTiO$_3$*, Appl. Phys. Lett. 94 (2009), 081903.

[34] Y. Yvry, V. Lyahovitskaya, I. Zon, I. Lubomirsky, E. Wachtel, and A.L. Roytburd, *Enhanced pyroelectric effect in self-supported films of BaTiO$_3$ with polycrystalline macrodomains*, Appl. Phys. Lett. 90 (2007), 172905.

[35] N.A. Pertsev, G. Arlt, and A.G. Zembilgotov, *Prediction of a giant dielectric anomaly in ultrathin polydomain ferroelectric epitaxial films*, Phys. Rev. Lett. 76 (1996), pp. 1364–1367.

[36] N.A. Pertsev and V.G. Koukhar, *Polarization instability in polydomain ferroelectric epitaxial thin films and the formation of heterophase structures*, Phys. Rev. Lett. 84 (2000), pp. 3722–3725.

[37] J.N. Walsh, P.A. Taylor, A. Buckley, T.W. Darling, J. Schreuer, and M.A. Carpenter, *Elastic and anelastic anomalies in (Ca,Sr)TiO$_3$ perovskites: analogue behaviour for silicate perovskites*, Phys. Earth Planet. Inter. 167 (2008), pp. 110–117.

[38] P. Heitjans and S. Indris, *Diffusion and ionic conduction in nanocrystalline ceramics*, J. Phys.: Condens. Matter 15 (2003), pp. R1257–R1289.

[39] J. Maier, *Ionic-conduction in-space charge regions*, Prog. Solid State Chem. 23 (1995), pp. 171–263.

[40] N. Sata, K. Eberman, K. Eberl, and J. Maier, *Mesoscopic fast ion conduction in nanometre-scale planar heterostructures*, Nature 408 (2000), pp. 946–949.

[41] X. Guo, W. Sigle, and J. Maier, *Blocking grain boundaries in yttria-doped and undoped ceria ceramics of high purity*, J. Am. Ceram. Soc. 86 (2003), pp. 77–87.

[42] A. Aird, M.C. Domeneghetti, F. Mazzi, V. Fazzoli, and E.K.H. Salje, *Sheet superconductivity in WO$_{3-x}$: crystal structure of the tetragonal matrix*, J. Phys.: Condens. Matter 10 (1998), pp. L569–L574.

[43] A. Aird and E.K.H. Salje, *Sheet superconductivity in twin walls: experimental evidence of WO$_{3-x}$*, J. Phys.: Condens. Matter 10 (1998), pp. L377–L380.

[44] A. Aird and E.K.H. Salje, *Enhanced reactivity of domain walls in WO$_3$ with sodium*, Eur. Phys. J. B 15 (2000), pp. 205–210.

[45] F. Camara, J.C. Doukhan, and E.K.H. Salje, *Twin walls in anorthoclase are enriched in alkali and depleted in Ca and Al*, Phase Trans. 71 (2000), pp. 227–242.

[46] S.A. Hayward, E.K.H. Salje, and J. Chrosch, *Local fluctuations in feldspar frameworks*, Mineral. Mag. 62 (1998), pp. 639–645.

[47] S. Kustov, S. Golyandin, K. Sapozhnikov, E. Cesari, J. Van Humbeeck, and R. De Batist, *Influence of martensite stabilization on the low-temperature non-linear anelasticity in Cu-Zn-Al shape memory alloys*, Acta Mater. 50 (2002), pp. 3023–3044.

[48] Y.W. Chai, H.Y. Kim, H. Hosoda, and S. Miyazaki, *Interfacial defects in Ti-Nb shape memory alloys*, Acta Mater. 56 (2008), pp. 3088–3097.

[49] S. Kustov, J. Pons, E. Cesari, and J. Van Humbeeck, *Pinning-induced stabilization of martensite – part II. Kinetic stabilization in Cu-Zn-Al alloy due to pinning of moving interfaces*, Acta Mater. 52 (2004), pp. 3083–3096.

[50] J.I. Kim and S. Miyazaki, *Effect of nano-scaled precipitates on shape memory behaviour of Ti-50.9at.% Ni alloy*, Acta Mater. 53 (2005), pp. 4545–4554.

[51] K. Otsuka and X.B. Ren, *Mechanism of martensite aging effects and new aspects*, Mater. Sci. Eng. A 312 (2001), pp. 207–218.

[52] Z. Li, Z.A. Xiao, and Z. Xiao, *Structural transition of stabilized martensite in CuZnAl alloy*, Multi-Functional Materials and Structures, PTS 1 and 2, Advanced Materials Research Volume 47–50 (2008), pp. 499–502.

[53] V. Khovaylo, R. Kainuma, K. Ishida, T. Omori, H. Miki, T. Takagi, and A. Datesman, *New aspects of martensite stabilization in Ni-Mn-Ga high-temperature shape memory alloy*, Phil. Mag. 88 (2008), pp. 865–882.

[54] M. Calleja, M. Dove, and E.K.H. Salje, *Anisotropic ionic transport in quartz: the defect of twin boundaries*, J. Phys.: Condens. Matter 13 (2001), pp. 9445–9454.

[55] R.J. Harrison, S.A.T. Redfern, and E.K.H. Salje, *Dynamical excitation ad anelastic relaxation of ferroelastic domain walls in LaAlO₃*, Phys. Rev. B 69 (2004), 144101.

[56] R.J. Harrison, S.A.T. Redfern, and J. Street, *The effect of transformation twins on the seismic-frequency mechanical properties of polycrystalline $Ca_{1-x}Sr_xTiO_3$ perovskite*, Am. Mineral. 88 (2003), pp. 574–582.

[57] J.R. Lagraff and D.A. Payne, *Oxygen stoichiometry and mobility effects on daomain-wall motion in ferroelastic $YBa_2Cu_3O_{7-\delta}$*, Ferroelectrics 130 (1992), pp. 87–105.

[58] M. Calleja, M. Dove, and E.K.H. Salje, *Trapping of oxygen vacancies on twin walls of CaTiO₃: a computer simulation study*, J. Phys.: Condens. Matter 15 (2003), pp. 2301–2307.

[59] W.T. Lee, E.K.H. Salje, and U. Bismayer, *Influence of point defects on the distribution of twin wall widths*, Phys. Rev. B 72 (2005), 104116.

[60] E.K.H. Salje and W.T. Lee, *Atomic force microscopy – Pinning down the thickness of twin walls*, Nat. Mater. 3 (2004), pp. 425–426.

[61] D. Shilo, G. Ravichandran, and K. Bhattacharya, *Investigation of twin-wall structure at the nanometre scale using atomic force microscopy*, Nat. Mater. 3 (2004), pp. 453–457.

[62] E.K.H. Salje and H. Zhang, *Domain boundary and elastic softening in KMnF₃ and $KMn_{1-x}Ca_xF_3$*, J. Phys.: Condens. Matter 21 (2009), 035901.

[63] R. Groger, T. Lookman, and A. Saxena, *Defect-induced incompatibility of elastic strains: dislocations within the Landau theory of martensitic phase transformations*, Phys. Rev. B 78 (2008), 184101.

[64] G.L. Fan, K. Otsuka, X.B. Ren, and F.X. Yin, *Twofold role of dislocations in the relaxation behavior of Ti-Ni martensite*, Acta Mater. 56 (2008), pp. 632–641.

[65] F.J. Perez-Reche, L. Truskinovsky, and G. Zanzotto, *Training-induced criticality in martensites*, Phys. Rev. Lett. 99 (2007), 075501.

[66] F.J. Perez-Reche and E. Vives, *Spanning avalanches in the three-dimensional Gaussian random-field Ising model with metastable dynamics: field dependence and geometrical properties*, Phys. Rev. B 70 (2004), 214422.

[67] F.J. Perez-Reche, B. Tadic, L. Manosa, A. Planes, and E. Vives, *Driving rate effects in avalanche-mediated first-order phase transitions*, Phys. Rev. Lett. 93 (2004), 195701.

[68] G. Fan, Y. Zhou, K. Otsuka, X. Ren, K. Nakamura, T. Ohba, T. Suzuki, I. Yoshida, and F. Yin, *Effects of frequency, composition, hydrogen and twin boundary density on the internal friction of $Ti_{50}Ni_{50-x}Cu_x$ shape memory alloys*, Acta Mater. 54 (2006), pp. 5221–5229.

[69] G.L. Fan, Y.M. Zhou, K. Otsuka, and X. Ren, *Ultrahigh damping in R-phase state of Ti-Ni-Fe alloy*, Appl. Phys. Lett. 89 (2006), 161902.

[70] D. Shilo, A. Mendelovich, and V. Novak, *Investigation of twin boundary thickness and energy in CuAlNi shape memory alloy*, Appl. Phys. Lett. 90 (2007), 193113.

[71] E.K.H. Salje, H. Zhang, A. Planes, and X. Moya, *Martensitic transformation in Ni-Ti-Fe: experimental determination of the Landau potential and quantum saturation of the order parameter*, J. Phys.: Condens. Matter 20 (2008), 275216.

[72] E. Salje and B. Wruck, *Order parameter saturation at low temperatures – numerical results for displacive and O/D systems*, Ferroelectrics 124 (1991), pp. 185–188.

[73] E.K.H. Salje, B. Wruck, and H. Thomas, *Order-parameter saturation and low-temperature extension of Landau theory*, Z. Phys. B – Con. Mat. 82 (1991), pp. 399–404.

[74] J.C. Lashley, S.M. Shapiro, B.L. Winn, C.P. Opeil, M.E. Manley, A. Alatas, W. Ratcliff, T. Park, R.A. Fisher, B. Mihaila, P. Riseborough, E.K.H. Salje, and J.L. Smith, *Observation of a continuous phase transition in a shape-memory alloy*, Phys. Rev. Lett. 101 (2008), 135703.

[75] S.A. Hayward and E.K.H. Salje, *Low-temperature phase diagrams: non-linearities due to quantum mechanical saturation of order parameters*, J. Phys.: Condens. Matter 10 (1998), pp. 1421–1430.

[76] A.E. Jacobs, *Solutions of the square-rectangular martensitic-transformation*, Phys. Rev. B 31 (1985), pp. 5984–5989.

[77] J. Chrosch and E.K.H. Salje, *Temperature dependence of domain wall width in LaAlO₃*, J. Appl. Phys. 85 (1999), pp. 722–727.

[78] M. Yamamoto, K. Yagi, and G. Honjo, *Electron-microscopic studies of ferroelectric and ferroelastic $Gd_2(MoO_4)_3$.1. Gerneral features of ferroelectric domain-wall, antiphase boundary, and crystal defects*, Phys. Status Solidi A 41 (1977), pp. 523–534.

[79] C. Roucau, M. Tanaka, J. Torres, and R. Ayroles, *Electron-Microscope study of the structure related to the ferroelastic properties of lead phosphate $Pb_3(PO_4)_2$*, J. Microsc. 4 (1979), pp. 603–610.

[80] C. Boulesteix, B. Yangui, G. Nihoul, and A. Barret, *High-resolution and conventional electron-microscopy studies of repeated wedge microtwins in monoclinic rare-earth sesquioxides*, J. Microsc. 129 (1983), pp. 315–326.

[81] F. Tsai, V. Khiznichenko, and J.M. Cowley, *High-resolution electron-microscopy of 90-degrees ferroelectric domain boundaries in $BaTiO_3$ and $Pb(Zr_{0.52}Ti_{0.48})O_3$*, Ultramicroscopy 45 (1992), pp. 55–63.

[82] W. Zapart, *Domain walls structure as studied by EPR*, Ferroelectrics 291 (2003), pp. 225–240.

[83] J. Chrosch and E.K.H. Salje, *Thin domain walls in $Yba_2Cu_3O_{7-\delta}$ and their rocking curves An X-ray diffraction study*, Physica C 225 (1994), pp. 111–116.

[84] B. Wruck, E.K.H. Salje, M. Zhang, T. Abraham, and U. Bismayer, *On the thickness of ferroelastic twin walls in lead phosphate $Pb_3(PO4)_2$ – An X-ray diffraction study*, Phase Trans. 48 (1994), pp. 135–148.

[85] S.A. Hayward and E.K.H. Salje, *Displacive phase transition in anorthoclase: the 'Plateau effect' and the effect of T1-T2 ordering on the transition temperature*, Am. Mineral. 81 (1996), pp. 1332–1336.

[86] K.R. Locherer, J. Chrosch, and E.K.H. Salje, *Diffuse X-ray scattering in WO_3*, Phase Trans. 67 (1998), pp. 51–63.

[87] S.A. Hayward, J. Chrosch, E.K.H. Salje, and M.A. Carpenter, *Thickness of pericline twin walls in anorthoclase: an X-ray diffraction study*, Eur. J. Mineral. 8 (1996), pp. 1301–1310.

[88] A.M. Glazer, *Classification of tilted octahedra in perovskites*, Acta Cryst. B 28 (1972), p. 3384.

[89] H.D. Megaw, *Crystal structure of double oxides of the perovskite type*, Proc. Phys. Soc. London 58 (1946), p. 133.

[90] A.M. Glazer and H.D. Megaw, *Structure of sodium niobate (T2) at 600°C, and cubic-tetragonal transition in relation to soft-phonon modes*, Phil. Mag. 25 (1972), p. 1119.

[91] W.T. Lee, E.K.H. Salje, and U. Bismayer, *Domain-wall structure and domain-wall strain*, J. Appl. Phys. 93 (2003), pp. 9890–9897.

[92] W.T. Lee, E.K.H. Salje, and U. Bismayer, *Structure and transport properties of ferroelastic domain walls in a simple model*, Phase Trans. 76 (2003), pp. 81–102.

[93] W.T. Lee, E.K.H. Salje, and M.T. Dove, *Effect of surface relaxation on the equilibrium growth morphology of crystals: platelet formation*, J. Phys.: Condens. Matter 11 (1999), pp. 7385–7410.

[94] E. Bousquet, M. Dawber, N. Stucki, C. Lichtensteiger, P. Hermet, S. Gariglio, J.M. Triscone, and P. Ghosez, *Improper ferroelectricity in perovskite oxide artificial superlattices*, Nature 452 (2008), p. 732.

[95] C.L. Jia, S.B. Mi, K. Urban, I. Vrejoiu, M. Alexe, and D. Hesse, *Atomic-scale study of electric dipoles near charged and uncharged domain walls in ferroelectric films*, Nat. Mater. 7 (2008), pp. 57–61.

[96] Y. Ishibashi, M. Iwata, and E. Salje, *Polarization reversals in the presence of 90 degrees domain walls*, Jpn J. Appl. Phys. 44(1) (2005), pp. 7512–7517.

[97] Y. Ishibashi and E. Salje, *A theory of ferroelectric 90 degree domain wall*, J. Phys. Soc. Jpn 71 (2002), pp. 2800–2803.

[98] A. Recnik, J. Bruley, W. Mader, D. Kolar, and M. Ruhle, *Structural and spectroscopic investigation of (111) twins in Barium-Titanate*, Phil. Mag. B 70 (1994), pp. 1021–1034.

[99] S. Stemmer, S.K. Streiffer, F. Ernst, and M. Ruhle, *Atomistic structure of 90-degree domain-walls in ferroelectric PbTiO$_3$ thin films*, Phil. Mag. A 71 (1995), pp. 713–724.

[100] G. Le Rhun, I. Vrejoiu, and M. Alexe, *Piezoelectric response hysteresis in the presence of 90 degrees domain walls*, Appl. Phys. Lett. 90 (2007), 012908.

[101] Y.M. Gufan and E.S. Larin, *Theory of 2 order parameter phase-transitions*, Fiz. Tverd. Tela 22 (1980), pp. 463–471.

[102] Y.M. Gufan and V.I. Torgashev, *On the phenomenological theory of many-component order parameter change*, Fiz. Tverd. Tela 22 (1980), pp. 1629–1637.

[103] J.F. Blackburn and E.K.H. Salje, *Sandwich domain walls in cordierite: a computer simulation study*, J. Phys.: Condens. Matter 11 (1999), pp. 4747–4766.

[104] E. Salje, *Thermodynamics of sodium feldspar I: order parameter treatment and strain induced coupling effects*, Phys. Chem. Minerals 12 (1985), pp. 93–98.

[105] E. Salje, V. Devarajan, U. Bismayer, and D.M.C. Guimaraes, *Phase-transitions in Pb$_3$(P$_{1-x}$As$_x$O$_4$)$_2$-Influence of the central peak and flip mode on the Raman-scattering of hard modes*, J. Phys. C – Solid State 16 (1983), pp. 5233–5243.

[106] E. Salje and V. Devarajan, *Potts-model and phase-transition in lead phosphate Pb$_3$(PO$_4$)$_2$*, J. Phys. C – Solid State 14 (1981), pp. 1029–1035.

[107] B. Houchmanzadeh, J. Lajzerowicz, and E.K.H. Salje, *Order parameter coupling and chirality of domain walls*, J. Phys.: Condens. Matter 3 (1991), pp. 5163–5169.

[108] E. Salje, *Kinetic rate laws as derived from order parameter theory 1. Theoretical concepts*, Phys. Chem. Minerals 15 (1988), pp. 336–348.

[109] E. Salje, B. Palosz, and B. Wruck, *Insitu observation of the polytypic phase-transition 2H-12R in PbI2 – investigations of the thermodynamic, structural and dielectric properties*, J. Phys. C – Solid State 20 (1987), pp. 4077–4096.